JOURNAL OF SOLID STATE CHEMISTRY **129,** 231–241 (1997)
ARTICLE NO. SC967231

Three NiAs–Ni_2In Type Structures in the Mn–Sn System

Margareta Elding-Pontén,* Lars Stenberg,* Ann-Kristin Larsson,*,[1] Sven Lidin,† and Kenny Ståhl‡

*Inorganic Chemistry 2, Center for Chemistry and Chemical Engineering, Lund Institute of Technology, P.O. Box 124, S-221 00 Lund, Sweden; †Inorganic Chemistry, Arrhenius Laboratory, Stockholm University, S-106 91 Stockholm, Sweden; and ‡Institut før Kemi, Bygning 207, DTU, DK-2800 Lyngby, Denmark

Received February 28, 1996; in revised form September 30, 1996; accepted October 10, 1996

The *B*8-type structure field of the Mn–Sn system has been investigated. Two high temperature phases (HTP1 and HTP2) and one low temperature phase (Mn_3Sn_2) were found. They all crystallize with the NiAs structure type with part of the trigonal bipyramidal interstices filled by manganese atoms in an ordered manner. The ordering as well as the manganese content is different for the three phases, giving rise to three different orthorhombic superstructures. Mn_3Sn_2 seems to have the lowest manganese content, since the corresponding basal unit cell is smaller than for HTP1-2. Structural models of the phases are based on selected area electron diffraction, X-ray powder diffraction, and preliminary single crystal X-ray measurements. The ideal cell parameters found are ($a = 7a_{hex}$, $b = \sqrt{3}a_{hex}$, $c = c_{hex}$), ($a = 5a_{hex}$, $b = \sqrt{3}a_{hex}$, $c = c_{hex}$), and ($a = 2a_{hex}$, $b = \sqrt{3}a_{hex}$, $c = c_{hex}$) for HTP1, HTP2, and Mn_3Sn_2, respectively. The crystal structure of Mn_3Sn_2 has been refined by means of the Rietveld method from X-ray powder diffraction data. Mn_3Sn_2 is orthorhombic, *Pnma*, $a = 7.5547(2)$, $b = 5.4994(2)$, $c = 8.5842(2)$ Å, $Z = 4$. (*Pbnm* in the setting above.) The compound is isostructural with Ni_3Sn_2 and γ'-Co_3Sn_2 (H. Fjellvåg and A. Kjekshus, *Acta Chem. Scand. A* 40, 23–30 (1986)). Final $R_p = 8.97\%$, $R_{wp} = 11.44\%$, GOF = 2.86, and $R_{Bragg} = 4.11\%$ using 43 parameters and 5701 observations and 330 Bragg reflections.

INTRODUCTION

In the *B*8-type structure field of the Mn–Sn system at least three different phases appear. They all have a composition in between that of the NiAs ($B8_1$) structure type and that of the Ni_2In ($B8_2$) structure type.

NiAs itself is hexagonal ($P6_3/mmc$, $a = 3.622$ Å and $c = 5.013$ Å) (2) and can be described as a close-packed array of arsenic atoms where the nickel atoms occupy all the octahedral interstices. In the structure there are also trigonal bipyramidal interstices which are all empty. If they are all filled, the Ni_2In structure type appears.

Structures with an intermediate composition are known to exist in many *T*–*B* systems, where *T* is a transition metal and *B* an element from the boron, carbon, nitrogen, or oxygen group (3, 4). These structures sometimes have an ordered partial occupancy of the trigonal bipyramidal interstices, resulting in superstructures. This ordering is often difficult to examine by X-ray methods, since twinning of the structures frequently occurs. By selected area electron diffraction (SAED), however, a supercell may easily be detected in the small single domains found in the crystals.

All of the *B*8-type structures of the Mn–Sn system have an intermediate composition. The structures have previously been described as one high temperature phase crystallizing with the hexagonal base cell ($a = 4.398$ Å and $c = 5.516$ Å) and one low temperature phase crystallizing with a hexagonal supercell with $\mathbf{a}' = 3\mathbf{a}$ (5). Both phases are reported to have the same composition, namely $Mn_{1.77}Sn$ (5) or $Mn_{1.74}Sn$ (6). In the literature the phases are also denoted by Mn_2Sn or $Mn_{2-x}Sn$.

EXPERIMENTAL

Manganese powder (Goodfellow Metals, 99.9%) and tin grains (Kistner, 99.5%) were pressed into pellets in desired proportions under a pressure of 10 ton/cm^2. The pellets were arc melted under argon, sealed under vacuum in silica tubes, and annealed at different temperatures. After annealing the tubes were quenched in ice water. The annealing temperatures used in the experiments were 450°C and 600–650°C for the low and high temperature phases, respectively. The annealing times were at least 1 week. Prolonged annealing (up to 3 months) produced no new effects.

The best initial composition for making the Mn–Sn *B*8-type structures was between 33 and 40 at.% tin. This is in good agreement with the phase diagram of the Mn–Sn system (7), where the *B*8-type structure range is between 31 and 38 at.% tin. With lower tin content much Mn_3Sn appeared in the X-ray powder patterns and with higher tin content much $MnSn_2$ together with Sn appeared.

[1]Present address: Research School of Chemistry, Australian National University, ACT 0200, Australia.

0022-4596/97 $25.00

All samples were primarily analyzed by powder X-ray diffraction (Guinier–Hägg camera with monochromated Cu$K\alpha$ radiaton and a film detector) for identification of the known phases (Sn, $MnSn_2$, Mn_3Sn, and Mn) and the *B*8-type structure phases. The difficulty in analyzing the *B*8-type phases by powder X-ray diffraction only is that the superstuctures are hard or impossible to observe unless there is a distortion of the base cell. This is due to the small domains in the samples. The hexagonal twinning makes the base reflections very strong compared to the possible superstructure reflections. In addition there is a very high absorption by the samples of the Cu$K\alpha$ X-ray, which makes the discovery of the superstructure reflections still more difficult. For a thorough examination of the *B*8-type structure phases SAED was applied using a JEOL 2000FX electron microscope with an energy dispersive X-ray (EDX) spectrometer (LINK AN1000) attached. This revealed three different supercells of which two are high temperature phases (HTP1 and HTP2) and one is a low temperature phase (Mn_3Sn_2). In addition to powder X-ray diffraction and SAED, single crystal X-ray measurements were made on a Nicolet *P*3*m* diffractometer (upgraded by Svensson and Sommarin, 1993 (8)) with a graphite monochromator and Cu$K\alpha$ radiation, or on an Enraf–Nonius CAD4 diffractometer with a graphite monochromator and Mo$K\alpha$ radiation. A powder pattern of Mn_3Sn_2 was collected with a Philips PW3710 powder diffractometer and refined by the Rietveld method. Theoretical calculations of both diffraction patterns using EMS (9) and X-ray powder patterns were made using the program Lazy-Pulverix (10).

COMPOSITION DEPENDENCE OF THE PHASES

The equilibrium composition of the phases is hard to ascertain. Single phase samples are difficult to prepare, and within twinned crystals high and low temperature modifications may coexist. Microprobe analyses by EDX show that the Mn content is about 60–65 at.%, but the different phases are not distinguishable because of the very similar composition. The Rietveld refinement of Mn_3Sn_2 reveals the Mn content in this phase to be exactly 60 at.%. Definitive elucidation of the compositions of the other two phases will require chemical analysis of a single (twinned) crystal specimen. However, the larger basal unit cell of HTP1–2 may be taken as an indication of higher Mn content for these phases than for Mn_3Sn_2.

Tin grows from all samples containing $MnSn_2$. While the as-synthesized samples show only traces of free tin on the outside of the ingots, this element is expelled from the ingot at all annealing temperatures. At room temperature tin grows as long, thin needles from all $MnSn_2$-containing samples. Especially for the low temperature samples this is very apparent. For the high temperature samples only a few needles were observed after months at room temperature. X-ray powder patterns from a synthesis at 450°C at a composition of 66.7 at.% tin show only $MnSn_2$ and traces of Sn. After 4 months at room temperature many tin needles were observed, and the powder patterns showed a strong increase in the intensities of the tin lines relative to the $MnSn_2$ lines. Thus, it would appear that $MnSn_2$ is not a line-phase at elevated temperatures, but accomodates exess tin which is expelled from the structure at lower temperatures. This explains the occurrence of three phases (*B*8, $MnSn_2$, and Sn) in the tin-rich samples.

TEMPERATURE DEPENDENCE OF THE PHASES

Both HTP1 and HTP2 turn into Mn_3Sn_2 on annealing at low temperatures. The transition temperature varies between 500 and 600°C, depending on the initial composition of the samples. For example, at 30 at.% tin, only HTP were found together with Mn_3Sn after annealing for a week at 520°C, while at 37 at. % tin, both HTP and Mn_3Sn_2 were found together with Mn_3Sn after a week at 600°C. Thus, it seems as if a higher tin content moves the transition to a higher temperature (Fig. 1).

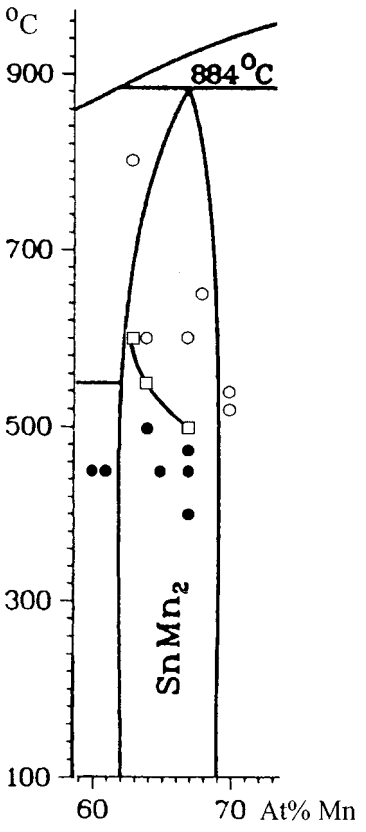

FIG. 1. Part of the phase diagram of the Mn–Sn system (7). ○ denotes the compositions at which the high temperature phases were found and ● the compositions at which the Mn_3Sn_2 was found. At □ at least one high temperature phase appeared together with Mn_3Sn_2.

Whether the phase transition temperature is the same for both high temperature phases or not, or if one of the high temperature phases first transforms to the other before Mn_3Sn_2 is formed, is still an open question. In a condensed electron beam, transitions occur from both high temperature phases to Mn_3Sn_2. Transition from one high temperature phase to the other has never been observed in the electron microscope.

DIFFRACTION

SAED

The SAED patterns very clearly show the superstructures as weak sattelite reflections in addition to the strong hexagonal base reflections. For all three phases the superstructure was observed along the $\langle 110\rangle^*_{hex}$ direction. In direct space this corresponds to either of the crystallographically equivalent $\langle 100\rangle_{hex}$ directions. All three superstructures could be ascribed orthorhombic cells. The transformation from a primitive hexagonal cell to an orthohexagonal C-centered cell may be expressed by the matrix pair

$$P = \begin{bmatrix} 1 & 1 & 0 \\ \bar{1} & 1 & 0 \\ 0 & 0 & 1 \end{bmatrix} \qquad P^{-1} = \begin{bmatrix} 1/2 & 1/2 & 0 \\ \overline{1/2} & 1/2 & 0 \\ 0 & 0 & 1 \end{bmatrix}.$$

The magnitudes of the direct cell axes are given by the relations $a_{ort} = a_{hex}$, $b_{ort} = \sqrt{3}a_{hex}$, and $c_{ort} = c_{hex}$.

The modulation vector $\mathbf{q}$ found for Mn_3Sn_2 in the SAED patterns (Fig. 2a) is

$$\mathbf{q}_{Mn_3Sn_2} = 1/4(\mathbf{a}^*_{hex} + \mathbf{b}^*_{hex}).$$

This vector is clearly equal to half $\mathbf{a}^*_{ort}$, and thus in direct space, the simple orthohexagonal cell is doubled along $\mathbf{a}_{ort}$.

The modulation vectors of HTP1–2 (Fig. 2b and 2c) are close to

$$\mathbf{q}_{HTP1} = 2/7(\mathbf{a}^*_{hex} + \mathbf{b}^*_{hex})$$

and

$$\mathbf{q}_{HTP2} = 3/10(\mathbf{a}^*_{hex} + \mathbf{b}^*_{hex}),$$

respectively. The elongation of the orthohexagonal base cell is in the same direction as for Mn_3Sn_2, however, by a factor of 7 for HTP1 and 5 for HTP2. The modulation vectors for these two phases are very similar; $2/7 \approx 0.29$ and $3/10 = 0.30$. Both HTP phases are slightly incommensurate.

The three orthorhombic cells have the ideal cell parameters

$$a_{Mn_3Sn_2} = 2a_{hex} \qquad a_{HTP1} = 7a_{hex} \qquad a_{HTP2} = 5a_{hex}$$

$$b_{Mn_3Sn_2} = \sqrt{3}a_{hex} \qquad b_{HTP1} = \sqrt{3}a_{hex} \qquad b_{HTP2} = \sqrt{3}a_{hex}$$

$$c_{Mn_3Sn_2} = c_{hex} \qquad c_{HTP1} = c_{hex} \qquad c_{HTP2} = c_{hex}.$$

The transformation matrices from the primitive hexagonal cell to the orthorhombic cells are

$$P = \begin{bmatrix} 2 & 2 & 0 \\ \bar{1} & 1 & 0 \\ 0 & 0 & 1 \end{bmatrix} \qquad P = \begin{bmatrix} 7 & 7 & 0 \\ \bar{1} & 1 & 0 \\ 0 & 0 & 1 \end{bmatrix} \qquad P = \begin{bmatrix} 5 & 5 & 0 \\ \bar{1} & 1 & 0 \\ 0 & 0 & 1 \end{bmatrix}$$

for Mn_3Sn_2, HTP1, and HTP2, respectively.

Powder X-Ray Diffraction

In the X-ray powder patterns, HTP1–2 were not distinguishable from each other. No superstructure lines were discernible and the patterns could be indexed with the hexagonal base cell, which was refined to $a = 4.3735(10)$ Å and $c = 5.5148(11)$ Å. A comparison of the intensities of the peaks showed that the 110 and 101 reflections were almost equal in intensity. In a hypothetic Mn_2Sn having the Ni_2In-type structure the 110 reflection is the strongest, and in a hypothetic MnSn having the NiAs-type structure it is the 101 reflection instead (Fig. 3). This indicates that the surplus Mn atoms indeed occupy positions equivalent to those of Ni2 in Ni_2In, i.e., the trigonal bipyramidal interstices. The same intensity distribution was observed for Mn_3Sn_2. This phase was, however, orthorhombically distorted and could therefore be distinguished from the high temperature phases. The distortion was observed as a split of some of the lines in the hexagonal base cell. In addition, some extra reflections appeared and most of the lines were moved toward higher 2θ values (Figs. 3c and 4).

From the X-ray powder patterns the orthorhombic cell of Mn_3Sn_2 was determined using the program PIRUM (11), the SAED patterns being used as an extra check. The orthorhombic cell, without the orthorhombic distortion, is $a_{ort} = 2a_{hex} = 8.7470$ Å, $b_{ort} = \sqrt{3}a_{hex} = 7.5751$ Å, $c_{ort} = c_{hex} = 5.5148$ Å, while the cell found in the refinement was $a = 8.5752(12)$ Å, $b = 7.5497(10)$ Å, $c = 5.4996(6)$ Å corresponding to an orthorhombic distortion of 2% ($a/2 = 4.29$ Å, $b/\sqrt{3} = 4.36$ Å) and a 3% reduction in volume compared to the high temperature cell (*Pbnm* setting).

By annealing at low temperatures it is possible to produce Mn_3Sn_2 without the orthorhombic distortion. Annealing an HTP sample at 200°C for 2 months produced Mn_3Sn_2 with a powder pattern identical to that of HTP except for line

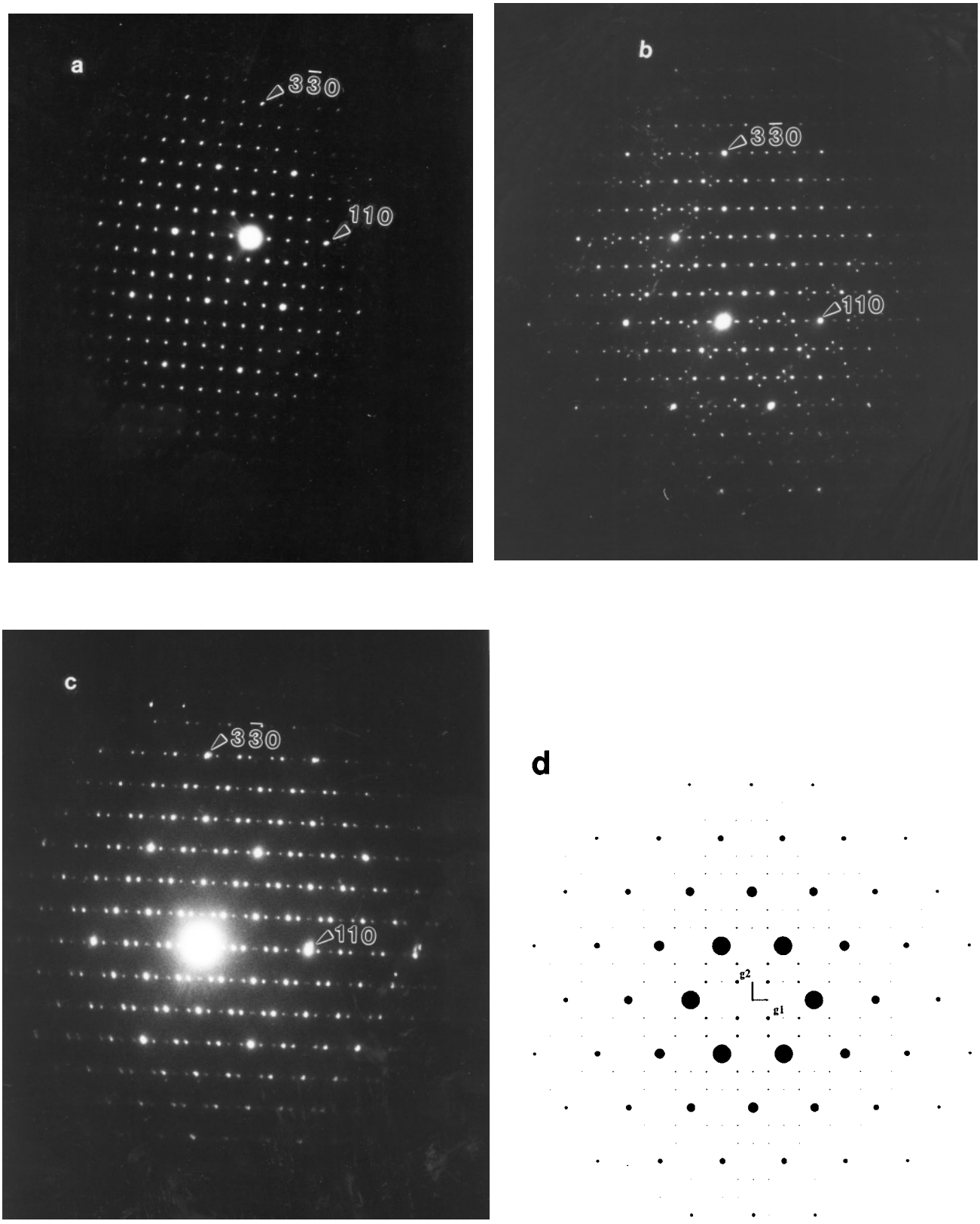

FIG. 2. SAED patterns of the *B*8-type Mn–Sn phases. The zone axis is $\langle 001 \rangle_{hex}$. The theoretical patterns were generated by EMS – V3.10a. Experimental pattern from (a) Mn_3Sn_2, (b) HTP1, and (c) HTP2, all indices refering to the hexagonal base cell. Theoretical pattern from the model of (d) Mn_3Sn_2, *Pnma* $\mathbf{g}1 = (001)_{ort}$ and $\mathbf{g}2 = (100)_{ort}$; (e) HTP1, *Cmcm* $\mathbf{g}1 = (100)_{ort}$ and $\mathbf{g}2 = (010)_{ort}$; and (f) HTP2, *Pnma* $\mathbf{g}1 = (001)_{ort}$ and $\mathbf{g}2 = (100)_{ort}$.

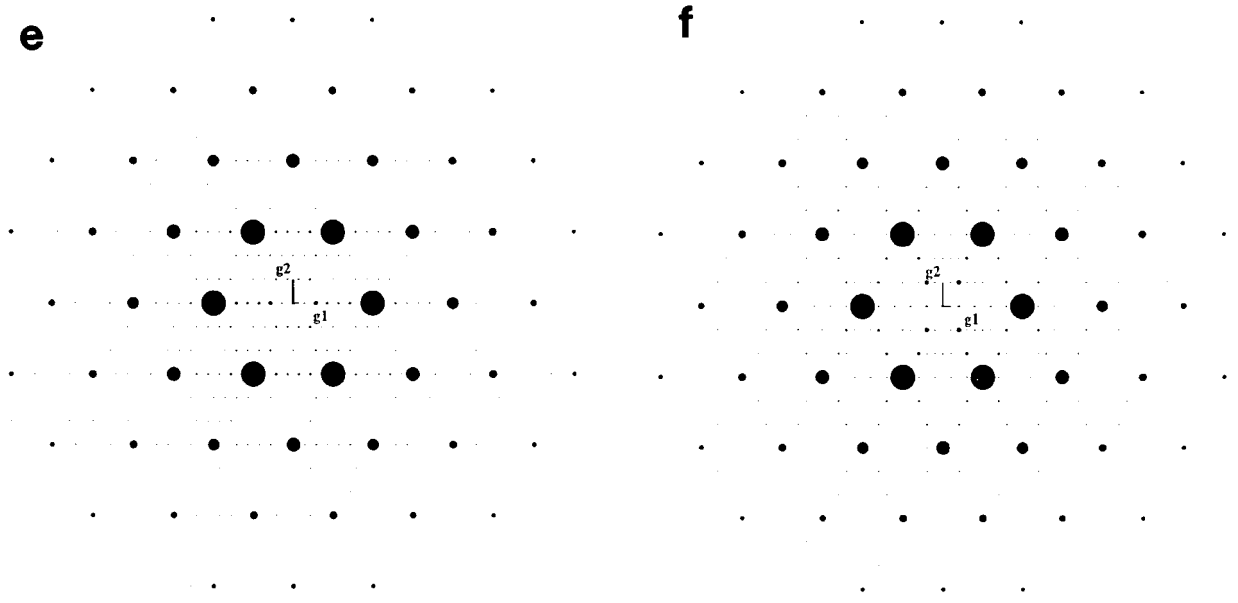

FIG. 2—*Continued*

broadening. Quasi-single crystal measurements revealed the additional reflections of Mn_3Sn_2 in a cell unaffected by orthorhombic distortion. This is consistent with the electron diffraction patterns, where Mn_3Sn_2 is observed both with and without the orthorhombic distortion.

High Resolution Transmission Electron Microscopy, HRTEM

Figure 5a shows the high and low temperature phases together in one crystal. The crystal is viewed along $\langle 0\,0\,1\rangle_{hex}$. Mn_3Sn_2 is seen as the light needle-shaped areas making a hexagonal array having angles of 60° and 120°. The darker areas are the HTP1. An enlargement of the marked area in Fig. 5a reveals the complicated structure in this crystal (Fig. 5b). Mn_3Sn_2 and HTP1 can be seen in this small domain.

STRUCTURAL MODELS

Structural determination of all of the three phases may be accomplished by X-ray or X-ray combined with electron diffraction. Preliminary single crystal X-ray work on HTP2 indicates that this is indeed a possible route. The preparation of high quality single crystals is, however, no simple task. From the limited information gathered so far, basic structural models for HTP1–2 have been constructed, taking symmetry information, SAED intensities, and the difference in the size of the basal unit cell into account, and the structure of Mn_3Sn_2 has been solved using the Rietveld method. HTP1–2 are both new types of superstructures. They are both effectively incommensurably modulated versions of the base structure, but the incommensurability is slight. Restricting the models to perfectly commensurate cases and assuming no partial occupancies, the indications from the SAED patterns are unambiguous.

Theoretical SAED patterns in different directions were compared with experimental patterns. Figures 2a–2f show the comparison in one of these directions, in which the zone axis is $\langle 0\,0\,1\rangle_{hex}$. Figure 6 shows the corresponding structural models.

In the calculations, HTP1 was assigned the orthorhombic space group *Cmcm*, matching the condition $h + k = 2n$ found from the SAED patterns, while for HTP2 *Pnma* was chosen, since preliminary single crystal X-ray measurements pointed toward this space group. Starting from a basic NiAs structure, MnSn, extra manganese atoms were inserted into the trigonal bipyramidal interstices. The symmetry allows 7 distinct models for HTP1 and 9 for HTP2.

Taking all the generated SAED patterns into account together with the EDX analysis of 60–65 at.% Mn, the structures in Fig. 6 seem to be the most probable. The manganese content for these models are 63.2 at.% for HTP1 ($Mn_{12}Sn_7$), 61.5 at.% for HTP2 (Mn_8Sn_5), and 60.0 at.% for Mn_3Sn_2. Satya Murthy *et al.* (6) found by neutron diffraction 2 Mn in Wyckoff position 2(*a*), 1.41 Mn in position 2(*d*), and 1.96 Sn in position 2(*c*) using the space group $P6_3/mmc$. This makes a manganese content of 63.5 at.% (or 63.0 at.% if there is 2 Sn in position 2(*c*)), which is very close to 63.2 at.% for HTP1.

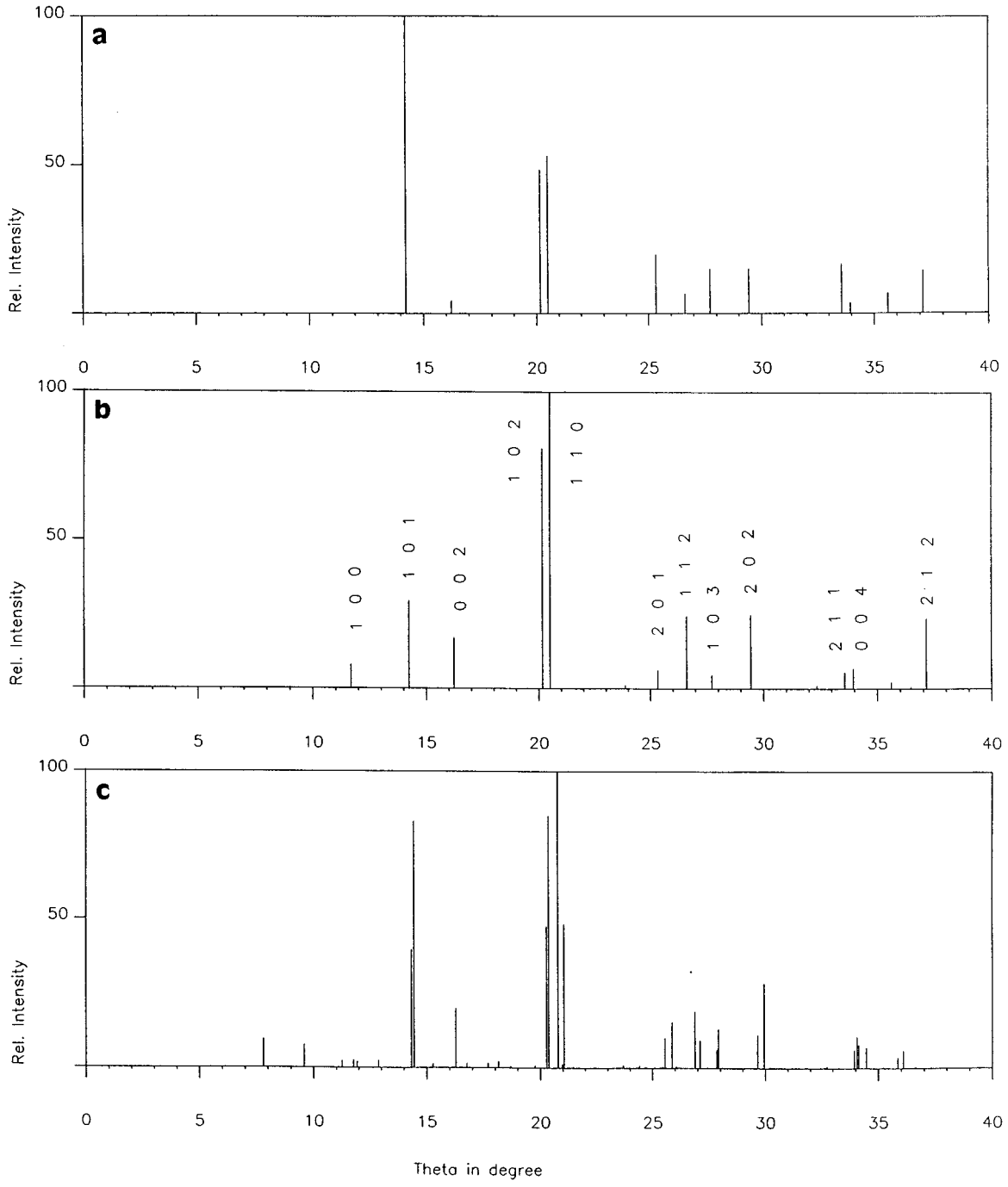

FIG. 3. Calculated X-ray powder patterns for compounds in the composition range MnSn–Mn_2Sn. Mn occupies the transition metal positions (Ni or Co) while Sn occupies the main group element position (As,Sn,In): (a) The hexagonal NiAs structure, $a = 4.398$ Å, $c = 5.516$ Å. (b) The hexagonal Ni_2In structure, $a = 4.398$ Å, $c = 5.516$ Å. (c) The orthorhombic Co_3Sn_2 (1) structure. The cell parameters have been modified to accomodate the orthorhombic distortion, $a = 7.550$ Å, $b = 5.500$ Å, $c = 8.575$ Å (space group *Pnma*).

RIETVELD REFINEMENT OF Mn_3Sn_3

Experimental

The synthesis of this powder was made according to the above description with an approximate initial tin to manganese atomic ratio of 2:3 (slight Sn excess *vide infra*). The sample was annealed at 650°C for 1 week and then at 450°C for another 4 weeks, after which the tube was quenched into ice water. One day after the quenching the tube was opened and the powder measurement was started.

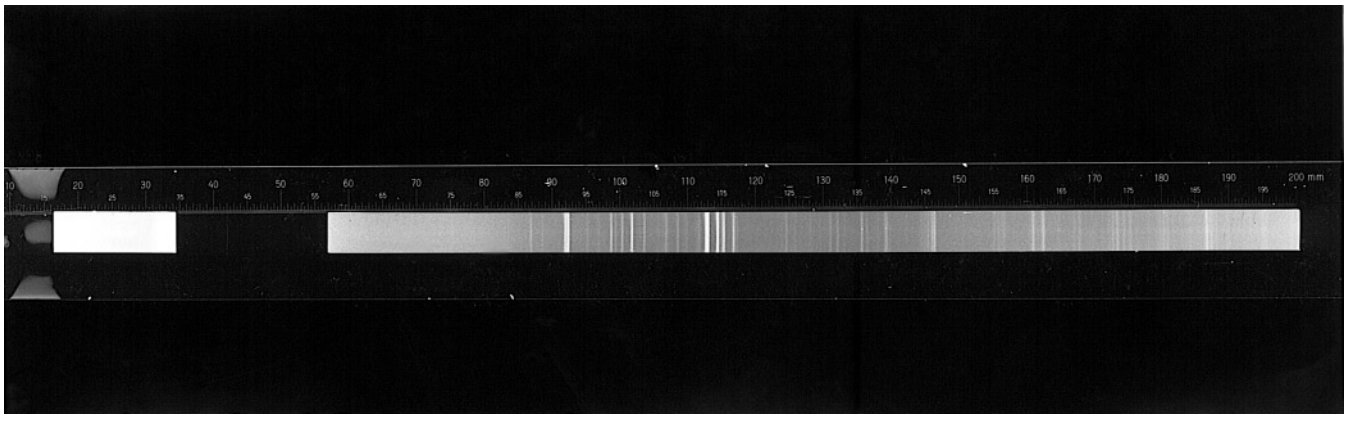

FIG. 4. Experimental X-ray powder pattern of Mn_3Sn_2 together with $MnSn_2$.

It was not possible to obtain single phase powder; all annealed samples contained either $MnSn_2$ or Mn_3Sn. As can be inferred from the phase diagram of the Mn–Sn system (7), $MnSn_2$ would be a line phase ($CuAl_2$-type structure), while Mn_3Sn (Ni_3Sn-type structure) shows a substantial solid solution field. Further, knowledge of the Mn_3Sn phase is scant. The published data contain several unindexed lines (12, 13), and it was judged expedient to use a slightly Sn-rich synthesis to get the more reliable $MnSn_2$ as a contaminant. The instability of $MnSn_2$ (e.g., expelling exess tin) at room temperature did not pose any major problems, as the measurement was carried out in a relatively short time.

The powder diffraction pattern was collected in reflection mode with a Philips PW3710 powder diffractometer, equipped with an auto-divergence slit and a stationary flat sample. The secondary graphite monochromator (after the sample instead of before the collimator) effectively eliminated the Mn-fluorescence background generated by the Cu$K\alpha$ radiation. The data set was collected between 5° and 130° in steps of 0.02° in 2θ, spending 13.25 s/step. The data set was corrected for the effect of the auto-divergence slit, and a separate file containing the corrected variances was generated and used for weighting in the subsequent Rietveld refinements. Reflections from both Cu$K\alpha$1 and Cu$K\alpha$2 are present. The Rietveld program takes this into account.

Refinement

The input cell parameters for the low temperature phase, Mn_3Sn_2, were 7.550, 5.500, and 8.575 Å as determined from the powder patterns. The space group was chosen as orthorhombic *Pnma*, as for γ'-Co_3Sn_2. The ideal cobalt and tin atomic positions of the γ'-Co_3Sn_2 structure were the input coordinates for manganese and tin, respectively (Table 1).

The Rietveld analysis (14) employed pseudo-Voigt profile functions, limited to 18 half widths, a Lorentzian component $y = y_1 + y_2(2\theta)$ and FWHM defined as $(V \tan\theta + W)^{1/2}$. The refinement also included the 2θ zero-point and 14 background parameters (Chebyshev type I). The structural parameters for Mn_3Sn_2 comprised one scale factor, three unit cell parameters, nine fractional coordinates and four isotropic temperature factor coefficients and those for $MnSn_2$ comprised one scale factor, two unit cell parameters, one fractional coordinate, two isotropic temperature factor coefficients, and one occupancy factor (Sn). The refinements were considered converged when all parameter shifts were less than 0.2 of the corresponding e.s.d. resulting in $R_p = 8.97\%$, $R_{wp} = 11.44\%$ and GOF = 2.86 from 5701 step intensities ($15° < 2\theta < 129°$) and 43 parameters. Final extracted $R_{Bragg} = 4.11\%$ from 330 reflections and $R_{Bragg} = 4.63\%$ from 67 reflections for Mn_3Sn_2 and $MnSn_2$, respectively. The refinement results have been summarized in Tables 1 and 2, and the diffraction pattern and final difference pattern is shown in Fig. 7.

The site occupancy factor (SOF) of Mn2 was refined to 0.5 within the standard deviation. Thus, the Mn2 site is fully occupied and the SOF was fixed to 0.5.

A few very small peaks (4) did not seem to be reduced at all in the refinement. These could be a product from the decomposition of $MnSn_2$. Including the Mn_3Sn phase into the refinement did not noticeably reduce the unidentified peaks.

Discussion/Results

This refinement verifies the structure indicated by the SAED and powder patterns.

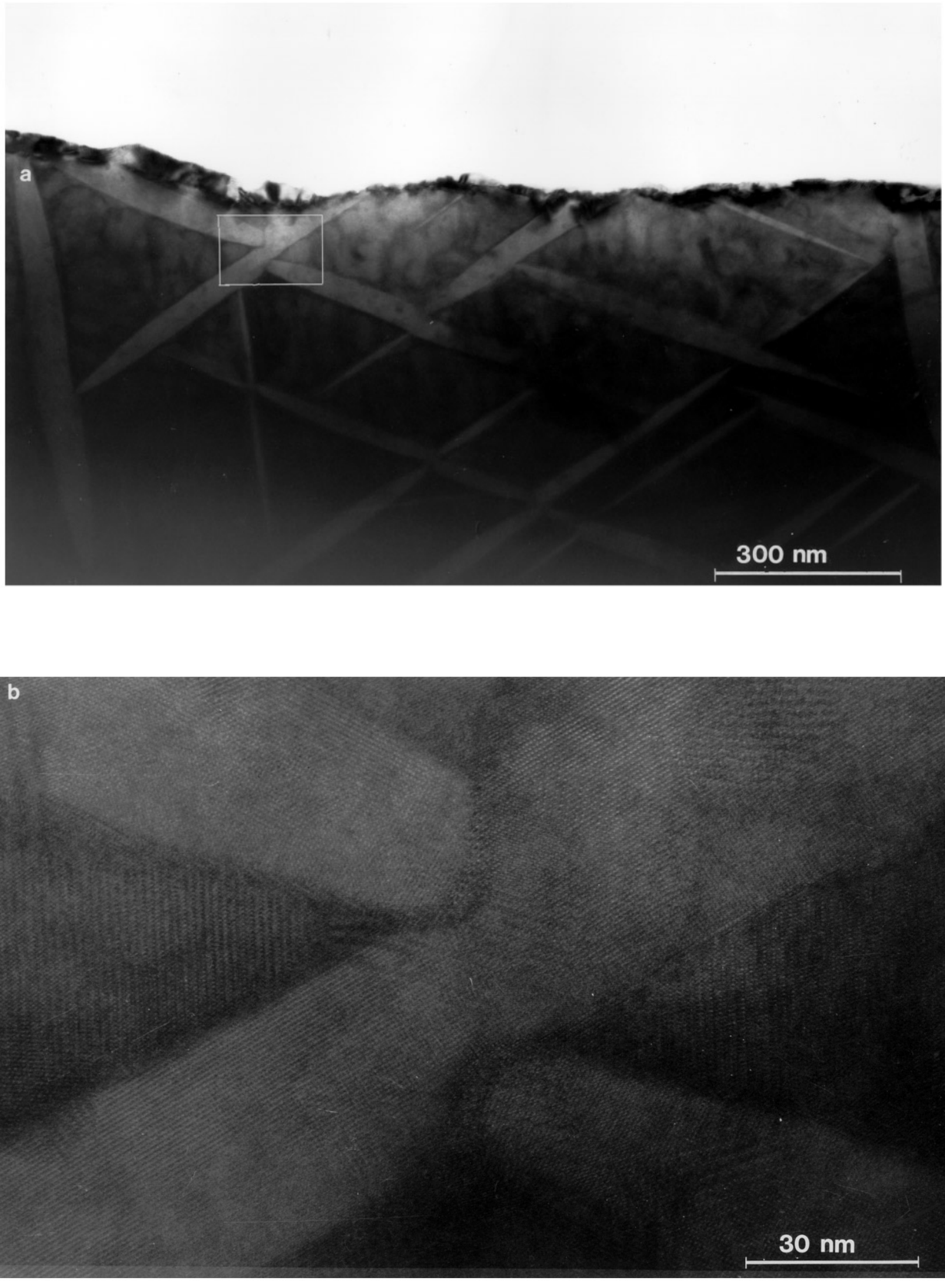

FIG. 5. HRTEM pictures of a crystal in the *B*8-type field of the Mn–Sn system.

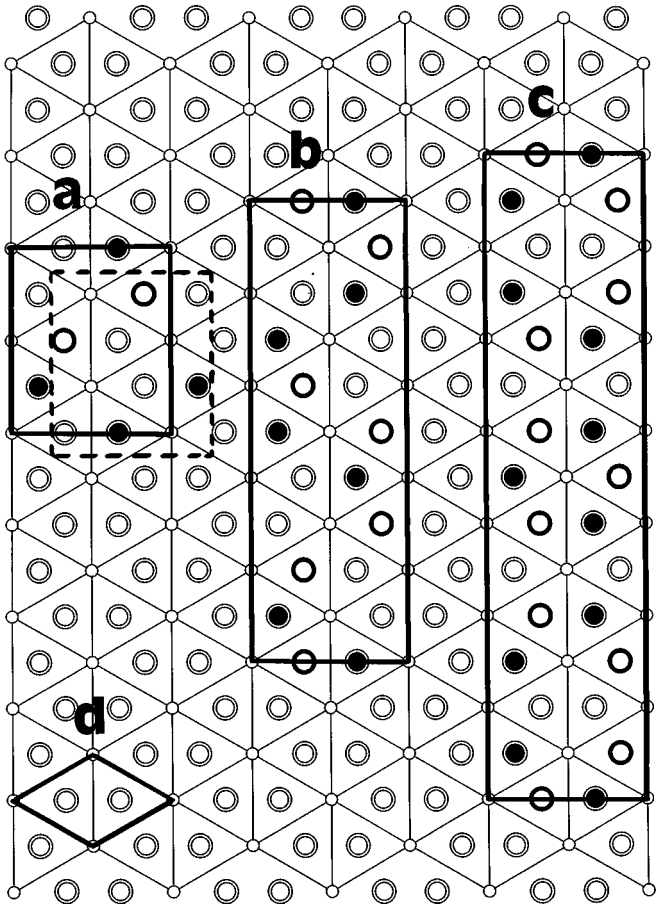

FIG. 6. Models of the *B*8-type Mn–Sn phases showing the extra Mn atoms in the trigonal bipyramidal interstices of the NiAs structure. The tin atoms are hexagonally close packed at heights 1/4 or 3/4, with manganese atoms (small circles at height 0 and 1/2) in all of the octahedral interstices. The extra manganese atoms (half-filled and filled larger circles) are located in the trigonal bipyramidal interstices of this NiAs-type structure. In the projection these positions coincide with the tin positions, however, displaced by 1/2 along the axis of projection. Half-filled circles correspond to Mn at height 1/4 and filled circles to Mn at height 3/4. (a) Mn_3Sn_2, *Pnma*. Dotted lines refer to the *Pnma* cell. (b) HTP2, Mn_8Sn_5, *Pnma*. (c) HTP1, $Mn_{12}Sn_7$, *Cmcm*. (d) The base NiAs-structure, $P6_3/mmc$.

TABLE 2
Distances in Å

Mn1	–	Mn1	2.689(7)
		Sn2	2.702(4)
		Mn2	2.762(5)
		Mn2	2.799(6)
		Mn1	2.811(7)
		Sn1	2.829(3)
		Sn1	2.856(4)
		Mn2	2.860(6)
		Sn2	2.882(3)
		Sn2	2.883(5)
		Sn1	3.048(4)
Mn2	–	Sn2	2.684(6)
		Sn1	2.697(5)
		Sn1	2.724(5)
		2Sn2	2.7582(4)
		2Mn1	2.762(5)
		2Mn1	2.799(6)
		2Mn1	2.860(6)
Sn1	–	Mn2	2.697(5)
		Mn2	2.724(5)
		2Mn1	2.829(3)
		2Mn1	2.856(4)
		2Mn1	3.048(4)
		2Sn1	3.255(2)
Sn2	–	Mn2	2.684(6)
		2Mn1	2.702(4)
		2Mn2	2.7582(4)
		2Mn1	2.882(3)
		2Mn1	2.883(5)

The structure of Mn_3Sn_2 may be described as a hexagonal close packing (Sn) with all octahedral interstices filled (Mn). The extra manganese atoms (Mn2) are situated in half of the trigonal bipyramidal interstices of the tin atom array. The bipyramids are deformed by Mn2 to get a larger

TABLE 1
The Atomic Input and Refined Values

Atom	Wyckoff position	*x* input	*x* refined	*y* input	*y* refined	*z* input	*z* refined	B_{iso} (Å^2) refined
Mn1[a]	8d	0.25	0.2305(4)	0	0.0056(6)	0.125	0.1320(5)	1.37(6)
Mn2[b]	4c	0.92	0.9114(6)	0.25	0.25	0.125	0.1208(6)	1.74(9)
Sn1	4c	0.58	0.5563(3)	0.25	0.25	0.125	0.0886(2)	1.83(5)
Sn2	4c	0.58	0.6024(3)	0.25	0.25	0.625	0.6429(3)	1.93(5)

Note. The tin atoms together make the hexagonal close packing.
[a]Mn1 is the manganese in all of the octahedral interstices.
[b]Mn2 is the extra manganese atom situated at the position of Sn2 + (0, 0.5, 0).

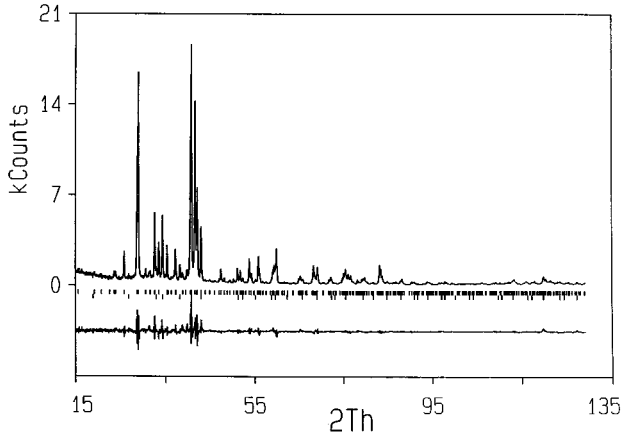

FIG. 7. Diffraction pattern and final difference pattern for Mn_3Sn_2 (and $MnSn_2$). Markers indicate $K\alpha 1$ Bragg positions for Mn_3Sn_2 (upper) and $MnSn_2$ (lower).

triangular base. These triangles are in the *ac* plane (*Pnma* setting) of the unit cell, which expands in this plane and contracts in the perpendicular direction (the *c* direction in the base hexagonal structure). The average hexagonal *c*/*a* value is 1.27 for Mn_3Sn_2 compared to 1.38 in pure NiAs (2), which has no atoms in the trigonal bipyramidal interstices, and $\sqrt{(8/3)} = 1.633$ for an ideal hexagonal close packing. For a pseudo-cubic structure the value is $\sqrt{(3/2)} = 1.225$. This corresponds to a compression along the hexagonal *c* axis (the *b* axis in Mn_3Sn_2) of the close packing that is so severe that the octahedra revert to truncated cubes (Fig. 8). This is the relation between ω-Ti and bcc described by Andersson (15). In Mn_3Sn_2 the hexagonal *c*/*a* ratio is close to this value, and the packing resembles that in bcc.

Because of the contraction along the *b* axis the coordination number of Mn2 becomes 11. Five of the atoms are the tin atoms of the trigonal bipyramid. The six additional atoms are Mn1, which together with the tin atoms are situated in the corners of an Edshammar polyhedron (16, 17).

The base coordination around Mn1 is octahedral by six tin atoms. Because of the above mentioned deformation of the octahedra there are also five manganese atoms close to Mn1. Two of these are Mn1, which together with the tin atoms are in the corners of an almost regular cube. This cube is capped on three faces by Mn2 atoms.

The base coordination around the tin atoms are six Mn1 in the corners of a trigonal prism. For Sn1 this prism is capped by Mn2 on two of the rectangular faces. These Mn2 atoms and two Sn1 atoms outside the prism form a large tetrahedron around Sn1. For Sn2 the trigonal prism is capped on one rectangular face and both triangular faces by Mn2.

Relative to the base hexagonal cell, Mn_3Sn_2 is orthorhombically distorted. This is also true for Ni_3Sn_2 but not for γ'-Co_3Sn_2 (1).

Although syntheses of Mn_3Sn_2 have been made with initial compositions ranging from 30 to 40 at.% tin, the cell parameters for properly heat treated samples of this phase are always found to be the same. The composition of Mn_3Sn_2 is thus most probably stoichiometric and independent of the starting composition. The lack of variation of the cell parameters indicates a line phase. This is compatible with γ'-Co_3Sn_2 but in contrast with Ni_3Sn_2, which shows strong dependence of the cell parameters with the occupation of the position corresponding to Mn2 (1).

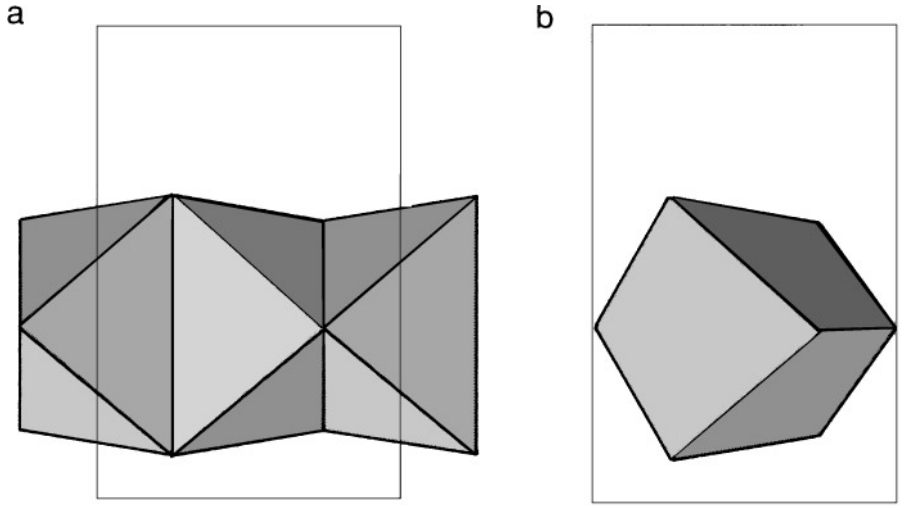

FIG. 8. Compression along the *b* axis (*Pnma* setting) in Mn_3Sn_2 (the hexagonal *c* axis). (a) Three truncated cubes as deformed octahedra shown in the *bc* plane. (b) A cube in the *bc* plane resulting from the deformation of the octahedra.

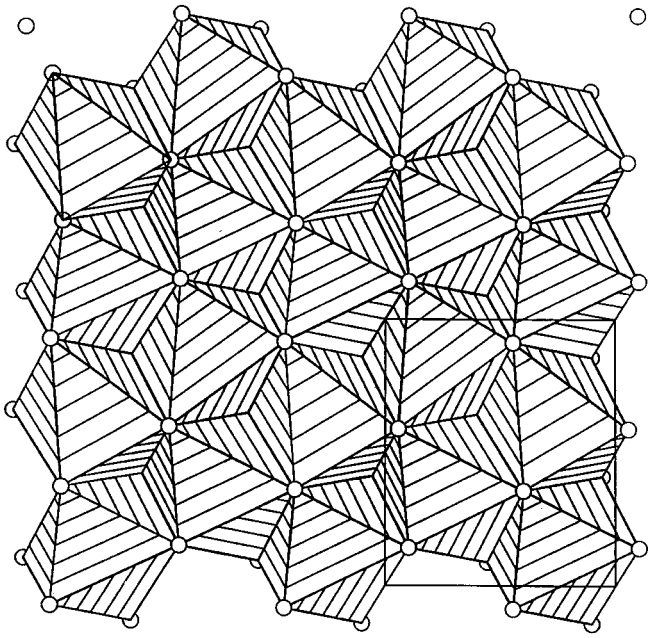

FIG. 9. The array of $MnSn_6$ octahedra shown in the *ac* plane.

The plot in Fig. 9 shows the $MnSn_6$ octahedra. The expansion of the base triangle of the triangular bipyramids between the octahedra is observed for half of the bipyramids. These are located at the positions of the Mn2 atoms.

CONCLUSION

Three different *B*8-type phases have been detected in the Mn–Sn system. Each was assigned an orthorhombic supercell. Structural models were made for these phases. The model of Mn_3Sn_2 was validated by means of the Rietveld method. Preliminary single crystal X-ray measurements confirmed the HTP2 model. For HTP1 the structural information from the experiments so far is insufficient to validate the proposed structural model. However, it is favored by the indications from the SAED patterns. The definitive answer to the question of the correct structures can only be provided by (single) crystal X-ray diffraction or by HRTEM coupled with image simulation. Work is in progress along these lines.

ACKNOWLEDGMENTS

Financial support from the Swedish Natural Science Research Council is gratefully acknowledged. We are grateful to Ms. Astrid Schøneberg for the powder data collection.

REFERENCES

1. Fjellvåg, H. and Kjekshus, A., *Acta Chem. Scand. A* **40,** 23–30 (1986).
2. "Powder Diffraction File," Report 31-900, JCPDS International Centre for Diffraction Data, PDF-2 Database, Version 2.12, Swarthmore, PA, 1991.
3. Lidin, S. and Larsson, A.-K., *J. Solid State Chem.* **118,** 313–322 (1995).
4. Villars, P. and Calvert, L. D., "Pearson's Handbook of Crystallographic Data for Intermetallic Phases," 2nd ed., Materials Park ASM, International cop., 1991.
5. Yasukochi, K. and Kanematsu, K., *J. Phys. Soc. Jpn.* **16(6),** 1123–1130 (1961).
6. Satya Murthy, N. S., Begum, R. J., Srinivasan, B. S., and Murthy, M. R. L. N., *Phys. Lett.* **15(3),** 225–227 (1965).
7. Massalski, T. B., "Binary Alloy Phase Diagrams", Am. Soc. Metals, Metals Park, OH, 1986.
8. Svensson, C. and Sommarin, B., *Acta Crystallogr. A* **49,** suppl. 20–20 (1993).
9. Stadelmann, P. A., *Ultramicroscopy* **21,** 131–146 (1987).
10. Yvon, K., Jeitschko, W., and Parthé, E., *J. Appl. Crystallogr.* **10,** 73–74 (1977).
11. Lundgren, J.-O., Report UUIC-B13-4-05, University of Uppsala, Sweden, (1982).
12. Nowotny, H. and Schubert, K., *Zeit. Für Metall.* **37,** 17–23 (1946).
13. Singh, U. P., Pal, A. K., Chandrasekaran, L., and Gupta, K. P., *Trans. Metall. Soc. AIME* **242,** 1661–1663 (1968).
14. Howard, C. J. and Hill, R. J., Australian Atomic Energy Commission Report M112, Lucas Hights Research Laboratory, New South Wales, Australia, 1986.
15. Andersson, S., *Arkiv Kemi* **15,** 247–252 (1960).
16. Edshammar, L.-E., Thesis, University of Stockholm, Sweden, 1969.
17. Lidin, S., Popp, T., Somer, M., and von Schneering, H. G., *Angew. Chem. Int. Ed. Engl.* **31,** 924–927 (1992).